Chapter 6

Measuring Single-Molecule Twist and Torque in Multiplexed Magnetic Tweezers

Franziska Kriegel, Willem Vanderlinden, Thomas Nicolaus, Angelika Kardinal, and Jan Lipfert

Abstract

Magnetic tweezers permit application of precisely calibrated stretching forces to nucleic acid molecules tethered between a surface and superparamagnetic beads. In addition, magnetic tweezers can control the tethers' twist. Here, we focus on recent extensions of the technique that expand the capabilities of conventional magnetic tweezers by enabling direct measurements of single-molecule torque and twist. Magnetic torque tweezers (MTT) still control the DNA or RNA tether's twist, but directly measure molecular torque by monitoring changes in the equilibrium rotation angle upon overwinding and underwinding of the tether. In freely orbiting magnetic tweezers (FOMT), one end of the tether is allowed to rotate freely, while still applying stretching forces and monitoring rotation angle. Both MTT and FOMT have provided unique insights into the mechanical properties, structural transitions, and interactions of DNA and RNA. Here, we provide step-by-step protocols to carry out FOMT and MTT measurements. In particular, we focus on multiplexed measurements, i.e., measurements that record data for multiple nucleic acid tethers at the same time, to improve statistics and to facilitate the observation of rare events.

Key words Single-molecule techniques, Magnetic tweezers, Multiplexing, Freely orbiting magnetic tweezers, Magnetic torque tweezers, DNA, Torque, Twist

1 Introduction

1.1 Magnetic Tweezers Apply Forces and Torques to Biological Macromolecules

Magnetic tweezers (MT) are a powerful technique to study the mechanical properties, dynamics, and conformational transitions of nucleic acids and to probe their interactions with proteins and other ligands [1–5]. In MT, molecules of interest are tethered between a flow cell surface and superparamagnetic beads (Fig. 1). Using permanent magnets or electromagnets, controlled stretching forces can be applied to the molecular tethers. In addition, rotation of the external magnetic field permits to rotate the magnetic particles in a controlled fashion and, therefore, systematically twist the molecular tethers, as first introduced by Strick et al. [5]. Conventional MT assays track the (x, y, z)-position of the magnetic beads

Yuri L. Lyubchenko (ed.), *Nanoscale Imaging: Methods and Protocols*, Methods in Molecular Biology, vol. 1814,
https://doi.org/10.1007/978-1-4939-8591-3_6,

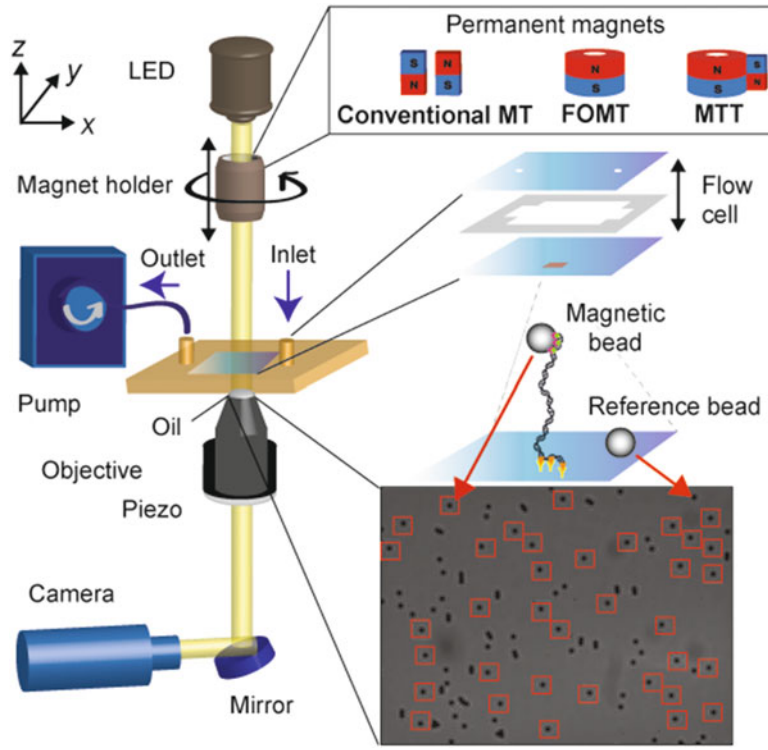

Fig. 1 Magnetic tweezers instrument. A flow cell is assembled from two glass cover slides (light blue on the right) that are separated by a Parafilm (light grey) layer that provides a measurement chamber. The flow cell is installed in a flow cell holder (light brown color) that is connected to a pump for fluid handling, and mounted on a stage to establish direct contact between the flow cell and an objective. The objective is placed on a piezo stage to control the focal plane, used in particular to sensitively calibrate the bead's *z*-position via their diffraction pattern. A LED monochromatically illuminates the sample through the magnet assembly and is directed via a mirror and a tube lens (not shown) to a camera, which is connected to a computer for read-out and bead tracking. A magnet holder, whose position in *z* and rotation around the vertical axis can be controlled by translation and rotation motors, is placed on top of the flow cell. Changing the magnet assembly changes the overall magnetic field, which in turn alters the force and the rotational trap stiffness applied to the magnetic beads (*see* also Fig. 2)

and apply stretching forces that are calibrated from transverse fluctuations [6–9]. MT have been applied to bare DNA (and RNA) to study nucleic acids upon overtwisting and undertwisting, or to probe mechanical properties, such as the bending persistence length or the stretch modulus [10–12]. In addition, MT have been used to study interactions of small molecules with DNA [13–15] and provided a platform to probe DNA– and RNA–protein interactions [4, 16–21] and processing. While conventional MT control the twist of the molecular tether, they do not track

rotation directly and do not measure torque. To overcome these limitations, recently new types of torque and twist measuring MT have been developed that are introduced in the next sections and that are the focus of this protocol paper.

1.2 Magnetic Tweezers for Twist and Torque Measurements: FOMT and MTT

Several variants of MT have been developed to enable direct measurements of torque and twist at the single-molecule level [2] (Fig. 2). Two main schemes can be distinguished. In freely orbiting magnetic tweezers (FOMT) and related approaches, one end of the molecular tether (typically DNA) can rotate freely, thus enabling measurements of angular changes within the DNA [22–25]. FOMT have enabled, for example, studying the assembly of nucleosomes on DNA [26] and resolved changes in the tether extension and the chiral winding of DNA in tetrasomes. Similarly, FOMT have been used to detect the assembly and helicity of nucleoprotein filaments involved in DNA repair formed by RecA [27] or Rad51 [28]. In a related assay, transcription of DNA by RNA polymerase [29] or the activity of DNA gyrase [23, 30] and the ensuing rotation of the DNA tether have been directly observed.

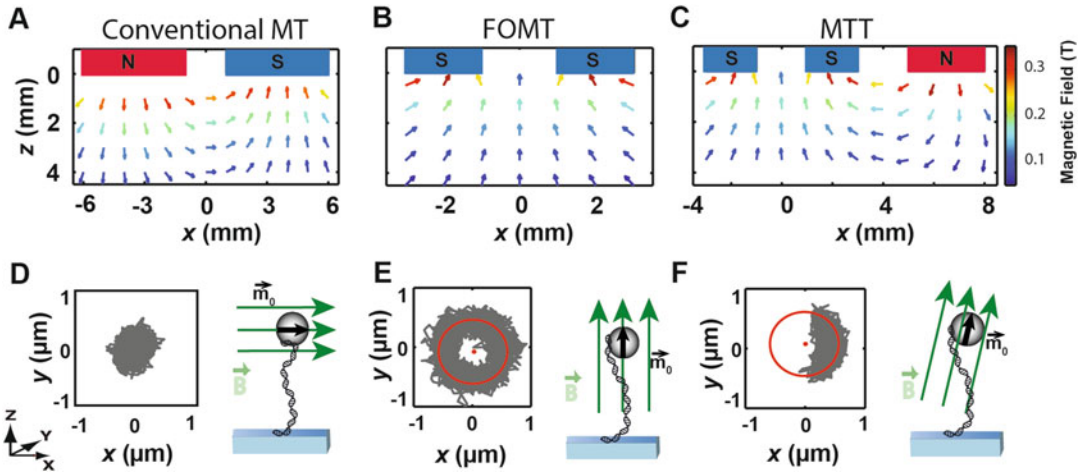

Fig. 2 Magnetic fields and bead fluctuations in conventional tweezers, FOMT, and MTT. Magnetic field calculations for conventional MT (**a**), freely orbiting magnetic tweezers (**b**), and magnetic torque tweezers (**c**). In conventional MT the bead's fluctuations in the (*x*, *y*)-plane are confined and trace out a small ellipse (**d**). The bead is free to rotate about the tether axis in FOMT, tracing out a doughnut-like pattern as illustrated in (**e**). The small side magnet in MTT adds a small horizontal field component such that the beads fluctuations are confined to an arc-like shape (**f**), i.e., in the MTT the bead does not trace out a full circle, but a segment of the doughnut, due to the rotational trap exerted in MTT by the magnets. Note that the bead aligns with the direction of the magnetic field $\vec{B}$ due to its preferred magnetization axis $\vec{m}_0$. In a typical FOMT or MTT experiment, initial assessment of tethered beads is performed using conventional MT magnets. Consequently, the geometry of the DNA–bead system in the flow cell is altered on changing to the FOMT or MTT magnet geometry (*see* also Fig. 4). Figure adapted from Ref. [54] with the permission from Elsevier Inc. Copyright© 2017 Elsevier Inc.

In magnetic torque tweezers (MTT) the twist of the molecular tether is still controlled by the external magnets, but the angular trap k_{ROT}, which is calibrated from the variance of the angular thermal fluctuations by $k_{ROT} = k_B \cdot T/\mathrm{Var}(\Theta)$ (where Θ is the rotation angle about the tether axis, k_B the Boltzmann constant, and T the absolute temperature), is weak enough to permit measurements of molecular torque from changes in the equilibrium angle $\langle\Theta\rangle$ [31–37] by $\tau = -k_{ROT} \cdot (\langle\Theta_N\rangle - \langle\Theta_0\rangle)$, where the subscript denotes the number of applied turns. MTT measurements have revealed the torsional stiffness of DNA and RNA as a function of applied stretching force [33, 38]. In addition, they have been used to probe, for example, the torsional response of DNA–-protein filaments [28, 33], nucleosomes [26, 31], and self-assembled DNA origami structures [37]. Basic aspects of how to perform MTT and FOMT measurements have been published in a video-based format previously [39].

Recently, torque measuring MT assays have been extended beyond simple molecular tethers to for example probe the torque generated by the bacterial flagellar motors in live cells [40–42]; however, here we focus on applications to DNA tethers in vitro.

1.3 Multiplexing Magnetic Tweezers

MT assays are used to address increasingly complex questions, e.g., involving several interaction partners in protein–nucleic acid interactions or nonprocessive reactions that are more demanding than "DNA only" measurements. The more complex the biological question, the more important is a reliable and robustly working instrument to perform precise measurements and to capture a maximum amount of data per measurement run. In addition, due to the relatively low torsional stiffness of ~kbp DNA tethers, molecular torque measurements even on bare DNA require measuring small angular deviations against thermal fluctuation noise, making it desirable to improve statistics beyond "one-molecule-at-a-time" measurements, again highlighting the need for parallelized measurements. Tracking of many beads in parallel in MT is possible (Fig. 1) and has been presented in earlier studies for conventional MT [43–45]. Recently, multiplexed measurements have also been demonstrated for MTT [46]. Multiplexed MTT have helped to increase statistics and have revealed the subtle changes in torsional stiffness of DNA upon variations in stretching force and salt concentration [46]. The multiplexed MTT measurements have resolved a small decrease (<10%) in the effective torsional stiffness of DNA for stretching forces smaller 2 pN at high salt concentrations (>500 mM NaCl or 10 mM $MgCl_2$), but found that the intrinsic torsional stiffness (at 6.5 pN stretching force) is independent of salt concentration. In addition, high-resolution multiplexed DNA torque measurements have enabled precise comparisons to coarse-grained simulations of DNA to test two mechanical models, the isotropic and the anisotropic rod model [46, 47].

Combining high-resolution torque measurements with simulations, the best fitting value for the intrinsic twist-bend coupling G was determined to be 40 ± 10 nm.

In this Chapter, we give detailed protocols on how to perform multiplexed magnetic torque tweezers measurements similar to the ones reported in Ref. [46, 47]. In addition, we provide guidelines for FOMT assays and demonstrate that FOMT measurements, too, can be carried out in a parallelized fashion.

2 Materials

2.1 Magnetic Tweezers Microscope

1. Torque measuring MT are currently only available as custom-built instruments. However, conventional MT instruments can be converted in a straightforward fashion to torque and twist measuring instruments by replacing the magnets and updating measurement and data analysis procedures. Here, we describe our implementation of a custom-made parallelized instrument.
2. A light emitting diode (Osram Oslon SSL, red, 612 nm) is used to illuminate the sample monochromatically from above.
3. An oil immersion objective (typically 60×, Plan Fluorite with correction collar, NA 0.9 or 40×, Plan Fluorite, NA 0.75, Olympus) is placed on a piezo (Pifoc, P-726.1CD and controller, E-753.1CD, Physik Instrumente) stage underneath the flow cell holder.
4. The flow cell holder is an important element used in MT to position and mount the flow cell onto the objective. It is (custom-) made of an aluminum (or steal) bottom holder and a top part made of PEEK (polyetheretherketon). The top part provides an inlet and outlet for fluid handling. The outlet is connected via an adapter (TECHLAB, VBM 101.538) to the tubing of the pumping system (*see* Subheading 2.1, **item 8**). The fluid system is sealed with rubber O-rings between the glass flow cell and flow cell holder.
5. The flow cell is imaged on the chip of a camera (Falcon PT-41-4M60, Dalsa) via a mirror (20D20ER.1, Newport) and tube lens (G322304000, Newport).
6. In conventional MT (Fig. 1), two cubic magnets ($5 \times 5 \times 5$ mm^3; W-05-N50-G, Supermagnete), separated by a small gap (typically 1 mm) are placed on a motorized arm and can be moved vertically using a translational motor (C-863.11-Mercury controller and M-126.PD2 motor, Physik Instrumente) and rotated with a rotation motor (C-863.11-Mercury controller and C-150.PD motor, Physik Instrumente).
7. The magnet arm itself is placed on two orthogonal translational micrometer-stages (M-UMR8.25, Newport) to precisely

control and align the relative position of the magnets main axis with the objectives main axis (*see* Subheading 3.5).

8. The flow cell outlet is connected to a peristaltic pump (ISM832C, Ismatec) for fluid handling [48].
9. The setup is controlled using a computer (DELL Precision T3600) equipped with a frame grabber (PCIe-1433, National Instruments) and using software written in LabVIEW (National Instruments) described by Cnossen et al. [45].
10. Measurements are generally performed at 60 Hz, but the acquisition frequency can be increased up to >1 kHz if a reduced field of view is used.

2.2 Magnetic Tweezers Software

1. In MT, the motion of the bead in the (x, y)- and z-position is tracked using the diffraction pattern of the bead, as described previously [6, 49].
2. Tracking is possible for many (>100) beads in parallel and carried out using the optimized routines described and made available by Cnossen et al. [45]. If necessary, the software allows tracking on GPUs for enhanced speed.

2.3 Flow Cells

Flow cells are constructed from a pair of glass microscope coverslips, separated by a parafilm spacer that is cut to form the flow channel with a scalpel. The top cover slide has two holes drilled with a laser cutter (*see* Subheading 3.2) to enable liquid exchange via an inlet and an outlet. The bottom cover slide is functionalized to bind digoxigenin-labeled DNA segments (*see* Fig. 1).

1. Coverslips: Glass cover slips 24 × 60 mm, No. 1, 130 μm thickness (Carl Roth).
2. Custom-made teflon holder for the preparation of clean glass cover slides.
3. (3-glycidoxypropyl)trimethoxysilane (abcr GmbH).
4. Parafilm M, 130 μm thickness (Carl Roth).
5. Anti-digoxigenin (Roche).
6. Bovine serum albumin (BSA) or BlockAid (BA) blocking solution (*see* Subheading 2.4, **item 3**).

2.4 Buffer Solutions

1. Phosphate-buffered saline (PBS) buffer to bind the DNA constructs to streptavidin-coated beads.
2. For nucleic acid measurements, we frequently employ Tris-EDTA (TE) buffer (1 mM EDTA and 10 mM Tris at pH 7.4) supplemented with varying concentrations of salt, e.g., NaCl or $MgCl_2$.
3. Solution of bovine serum albumin (BSA, ~25 mg/mL) and Tween (~0.1% v/v) or commercial available BlockAid blocking solution (ThermoFisher) to passivate the flow cell.

2.5 Superparamagnetic Beads

1. To couple DNA to magnetic beads we use streptavidin-coated, commercially available Dynabeads already functionalized with multiple streptavidin binding sides.
2. We generally use two types of beads (*see* **Note 1**): streptavidin-coated 1.0 μm diameter MyOne or 2.8 μm diameter M270 beads (Life Technologies).

2.6 DNA Constructs for Tweezers Measurements

1. pBluescript II SK plasmid (Stratagene).
2. Miniprep Kit (Qiagen).
3. Restriction enzymes (Xho1 and Pci1, NEB).
4. 10x Tango buffer solution (Thermo Fisher).
5. Monarch, Gel extraction kit (NEB).
6. λ-Phage DNA (NEB).
7. Primer sequence (for λ-phage DNA):

   Xho1-forward (5′AGTGGCTACGGCTCAGTTTG′3);
   Xho1-reverse (5′AACATTCGCTTATGCGGATTATTGC′3);
   Pci1-forward (5′CCGGCAATACTCGTAAACCATATCAA′3);
   Pci1-reverse (5′CCGCAGAGTGGATGTTTGAC3′).
8. dNTP mix (10 mM, ThermoScientific).
9. DMSO.
10. Taq DNA polymerase (NEB).
11. Biotin-16-dUTP (Sigma-Aldrich).
12. Digoxigenin-11-dUTP (Sigma-Aldrich).
13. 0.8 to 1%-high resolution agarose gels.
14. Ethidium bromide (EtBr; Sigma).
15. PCR purification kit (Qiagen).
16. Gel extraction Kit (Qiagen).
17. T4 DNA ligase (ThermoScientific).
18. Proteinase K (20 mg/mL, Biolabs).

3 Methods

3.1 Preparation of DNA Constructs

The aim is to construct DNA molecules with a specific length and sequence (the "middle part") and with multiple labels at each end ("handles") for MT measurements. Typically, one end is labeled with multiple biotin linkages to bind to streptavidin-coated magnetic beads and the other end is labeled with multiple digoxigenin moieties to bind specifically to anti-digoxigenin at the surface of the flow cell. We construct the three parts of DNA independently and then ligate them together to assemble: handle with biotin–middle part–handle with digoxigenin.

3.1.1 Middle Part

1. The plasmid containing the DNA sequence (pBluescript II SK) for the middle part is amplified in *E. coli* using standard protocols (*see* for example Ref. [50]). The plasmid DNA is purified using a Miniprep kit.
2. To generate linear, double-stranded DNA molecules we start with the plasmid (500 ng/μL) from which we generate a 7927 base pair long DNA strand by cutting with two restriction enzymes (Xho1 and Pci1) in Tango buffer solution simultaneously.
3. Run the restriction products on a 0.8% agarose gel in the absence of any DNA stain. To load large sample volumes (>50 μL), we create a large well by joining three protrusions of the gel comb using scotch tape. After electrophoresis, the gel is cut using a clean scalpel along the electrophoresis direction, and through the broad lane (at 0.5 cm from one edge) containing the sample. This procedure separates the gel along the broad sample lane into a smaller and a larger portion.
4. The smaller gel portion is stained by incubation in an aqueous EtBr solution. On a UV trans-illuminator, the product bands are visualized, and compared to a 1 kb DNA ladder run in an adjacent lane. The band containing the product at the expected length is excised and removed from the gel.
5. The smaller gel portion with excised product band is aligned to the larger, unstained gel portion. The position of the excised gel band in the small gel portion indicates the position of the desired restriction fragment in the larger (unstained) gel fraction. Excise the corresponding gel slice in the unstained larger gel portion with a clean scalpel. Use the gel extraction kit to extract DNA from the gel slice.
6. The overall yield of the restriction digest and subsequent purification steps, is ~40% (DNA concentration ~200 ng/μL).

3.1.2 Handles

We generate handles that have multiple bindings sides, either biotin or digoxigenin, by PCR from a λ-phage DNA template. We choose the biotin handle to bind to the Pci1 restriction side and the digoxigenin handle to bind to the Xho1 restriction side.

1. We use λ-phage DNA to (PCR-) generate DNA strands of approximately 700 base pairs with multiple biotin or digoxigenin-labels incorporated to bind to the magnetic beads (via the biotin:streptavidin linkages) and to the surface of the flow cell (via digoxigenin–anti-digoxigenin interactions).
2. For PCR we use 5 μL of reverse and forward primers (10 μM), 2 μL of dNTPs (10 mM), 5 μL of DMSO, 5 μL of λ-phage DNA (stock solution), 1 μL of Taq DNA polymerase, and 7.5 μL of labeled nucleotides at 1 mM concentration in a total volume of 100 μL.

3. We combine the Pci1 restriction side with the digoxigenin labels to construct DNA with 712 base pairs and Xho1 with biotin labels to construct DNA with 778 base pairs.
4. The restriction site can be a part of the λ-phage DNA sequence. If so, make sure that the primers produce a DNA strand with only one restriction site at the correct position.
5. If the desired restriction side is not part of the λ-phage DNA sequence, the sequence of the restriction enzyme can be included into the primer sequence (in this protocol the restriction sides are parts of the plasmid sequence).
6. To control the PCR products we run agarose gels using ~3 μL of the reaction volume.
7. The remaining volume of the PCR products is treated with a PCR cleanup kit and result in concentrations around ~40–70 ng/μL DNA.
8. Both of the labeled DNA fragments are cut using the same restriction enzymes as in Subheading 3.1.1, **step 2**. to generate single stranded DNA overhangs complementary to the 7927-base-pair-long middle part.
9. We use 30 μL of handle-DNA and 3 μL of Pci1 (or Xho1) in a total volume of 40 μL.
10. Incubate the restriction reaction overnight at 37 °C.
11. Afterward perform a "heat shock" at 65 °C for 10 min to degrade the restriction enzymes.
12. Use the PCR cleanup kit for each DNA construct (biotin labeled and digoxigenin labeled).
13. Final DNA concentrations are around 40 ng/μL.

3.1.3 Ligation

1. We ligate the middle construct with both handles in a ratio of 1:4:4 and try to maximize the concentration of DNA.
2. We use 8 μL of ligase in 139 μL overnight at 22 °C.
3. Heat-shock at 75 °C for 10 min to inactivate the ligase.
4. Use the whole amount of the ligated DNA construct and add Proteinase K (3 μL in a total volume of 157 μL) for 3 h at 37 °C.
5. Heat shock at 75 °C for 10 min to inactivate the Proteinase K.
6. The DNA construct is ready to use.
7. Aliquot the DNA preparation and store aliquots at −20 °C. After thawing, store the aliquot at +4 °C to avoid repeated freeze–thaw cycles. DNA remains useable for several months even at +4 °C.

3.2 Flow Cell Assembly

3.2.1 Top Glass Coverslips

1. We use a laser-cutter (Speedy 100, Trotec) to create holes of ~1 mm diameter on both sides of a glass coverslip at a distance of ~5 mm from the short edge for the top glass coverslips to serve as fluid inlets and outlets that match the dimensions of the flow cell holder.
2. To create the holes we use a power of 4.5 W, a laser with wavelength 1060 nm and a frequency of 1000 Hz.
3. The instrument provides software to create a layout from the glass coverslips to direct the laser to the desired positions.
4. It is best to probe several glass coverslips and optimize the layout file, as glass coverslips are cheap and the creation of two holes takes less than 1 min.
5. Top glass coverslips are sonicated in a 1:1 mixture of H_2Odd and 2-Propanol for 10 min before use.
6. Do not touch the flat surface of the coverslip. Coverslips can be touched at the edges.

3.2.2 Bottom Glass Coverslips

1. Install glass cover slides in teflon holder that is placed in a glass container, and sonicate in a 1:1 mixture of H_2Odd and 2-propanol for 10 min.
2. Next, the cover slides are treated with a 1:1 mixture of H_2SO_4 (concentrated) and H_2O_2 (30%) for 20 min.
3. Extensively rinse with H_2Odd.
4. Rinse cover slides with ethanol *p.a.*
5. Place cover slides in silane-solution (88% ethanol *p.a.*, 10% H_2O, 2% Silane ((3-glycidoxypropyl)-trimethoxy-silane) and incubate for 1 h.
6. Rinse with ethanol *p.a.*
7. Rinse with H_2Odd.
8. Dry in N_2 stream.
9. Heat for 45 min at 80 °C.
10. Store bottom glass cover slides under argon (ready to use, do not touch the binding side!).

3.2.3 Sealing the Flow Cell

Top and bottom glass cover slides are assembled with a single layer parafilm spacer (that is cut manually with a scalpel, like in our case, or using the laser cutter) on a heating plate for 1 min at 80 °C (*see* also Fig. 1 for the approximate pattern of the parafilm layer, light grey on the right).

3.2.4 Installing the Flow Cell to the MT Setup

Next, the assembled flow cell is placed into a flow cell holder and the flow cell assembly is mounted onto the oil objective of the instrument (*see* Fig. 1).

3.2.5 Flow Cell Surface Functionalization

Anti-digoxigenin at 100 μg/mL in PBS buffer is incubated for at least 1 h, followed by flushing the flow cell with PBS buffer (~600 μL, corresponding to >10 cell volumes).

3.2.6 Flow Cell Surface Passivation

To passivate the flow cell surface the chamber is filled with BlockAid or BSA-Tween solution (*see* Subheading 2.4). Before introducing the DNA–bead solution (*see* Subheading 3.3) the flow cell is rinsed with ~500 μL PBS buffer.

3.3 Preparation of DNA–Bead Solution and DNA Tethering

1. Measurements, shown within this work, were performed using the 7.9 kbp DNA construct described previously [33] and prepared as outlined in Subheading 3.1.
2. The DNA construct is first coupled to the streptavidin-coated beads (*see* **Note 2**) by incubating ~1 ng of the DNA construct with 2 μL of MyOne (or, alternatively, 5 μL M270) beads in a final volume of 20 μL PBS buffer for ~12 min (~5 min for M270 beads).
3. The DNA–bead solution is subsequently diluted into 100 μL PBS. The dilution needs to be adjusted for different DNA molecules or beads, such that the final surface coverage in the MT is optimized, i.e., to have enough useful beads to track, but not too many beads such that the diffraction pattern of the beads overlap.
4. Finally, 60 μL of the diluted DNA–bead solution, which corresponds to approximately one flow cell volume, are flushed into the flow cell at 170 μL/min.
5. After ~7 min (~40 s for M270 beads) unbound beads are removed by flushing with PBS buffer at 400 μL/min for at least 2 min (1 min for M270 beads).
6. Finally, the magnet holder with magnets in conventional MT geometry is mounted on the setup to apply stretching forces (~2 pN).
7. The DNA and bead concentrations and the bead-to-DNA ratio should be adjusted such that DNA-tethered beads are almost exclusively attached via single double-stranded DNA molecules. Lower the DNA concentration if many beads are attached via multiple DNA molecules. *See* the next sections on how to discriminate single from multiple tethers.
8. Typically, ~50–80% of the single DNA tethers in a flow cell can be supercoiled. The exact number depends on the quality of the DNA preparation and the length of the construct.

3.4 Tether Selection with Conventional MT

For initial selection of good DNA tethers, we use conventional MT magnets in a vertical configuration (Fig. 1), which exert a horizontally aligned magnetic field, as explained in Subheading 2.1, **item 6**.

To select for magnetic beads tethered to a single, torsionally constrained double-stranded DNA molecule, we perform three tests:

1. As a first test, we select DNA tethers that have (close to) the expected contour length. We check the tether length by varying the magnet distance to the flow cell from 0.5 mm to 12 mm, which corresponds to 4.4 pN and <0.1 pN, for MyOne beads, respectively and 55 pN to <0.1 pN for M270 beads, respectively. At a magnet height of 0.5 mm the DNA tethers are stretched to >95% of their contour length whereas at 12 mm (close to zero force) the beads drop the bottom surface, corresponding to zero tether extension. The expected tether length is 0.34 nm per base pair times ~7900 base pairs, equal to ~2700 nm. Beads with a tether length close to the expected contour length are further considered.
2. To select beads that are tethered by a single double-stranded DNA molecule, we take advantage of the asymmetric response of DNA upon underwinding and overwinding at stretching forces >1 pN (*see* also Fig. 3). We exert a pulling force of ~1.5 pN and turn the magnets 20 times against the helical orientation of DNA (clockwise). If the tether length decreases, we assume multiple molecules to be bound to that bead and discard them from further analysis.
3. Finally, we select DNA tethers that are fully torsionally constrained, which requires multiple attachment points at both ends and no nicks along the DNA molecule. We move the magnets to exert a stretching force of ~0.4 pN and rotate the magnets by ±20 turns. If there is a single, coilable DNA molecule attached to the bead the molecule buckles resulting in a decrease of the tether length (*see* also Fig. 3). Note, that the number of turns required will vary for longer (or shorter) DNA constructs. Only beads that pass all three tests are used for further analysis.

3.5 FOMT Alignment and Measurements

Having selected beads that are tethered by single, torsionally constrained DNA constructs, we replace the conventional magnet configuration by a stack of cylindrical magnets with a central aperture (R-06-02-02-G, N-45, Supermagnete) for FOMT measurements (Figs. 1 and 2). This stack consists of three ring magnets with an outer diameter of 6 mm, an inner diameter of 2 mm and a height of 2 mm per magnet (*see* **Note 3**). Magnets are not brought closer to the flow cell than 3 mm (*see* **Note 4**). For the force calibration and the analysis of the (x, y)-fluctuations in FOMT, measurements were performed at 3, 3.5, 4, 4.5, and 5 mm magnet height for 600 s for MyOne beads and 1200 s for M270 beads (*see* **Note 5**). FOMT measurements require precise alignment of the magnets relative to the flow cell, to achieve a situation where the

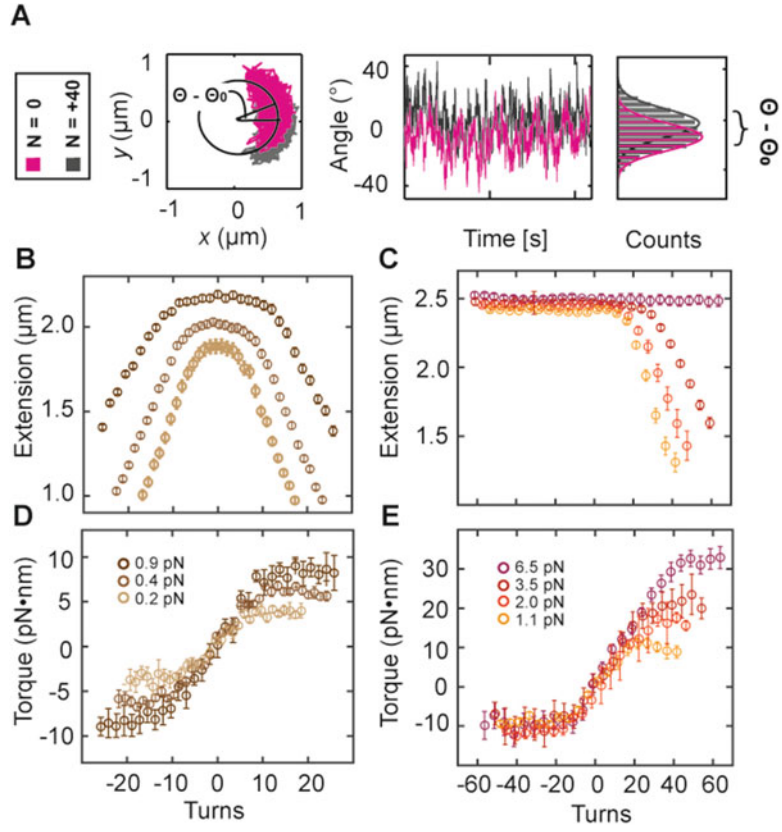

Fig. 3 Torque measurement for DNA. (**a**) Angular tracking in MTT. (x, y)-data are transformed to polar coordinates. The bead's position has an equilibrium angle Θ_0 for a torsionally relaxed tether (pink). The fluctuations around Θ_0 are a measure of the rotational trap stiffness k_{ROT}. The shift in the equilibrium angle Θ_0 after N turns to Θ (grey) can be converted to molecular torque. In MTT two signals are recorded at the same time: the tethers' extensions (**b**, **c**) and their molecular torque (**d**, **e**) upon the application of twist. The response of DNA to induced twist depends on the stretching force. (**b**, **d**) For forces smaller 1 pN, the response of DNA to twist is symmetric around zero turns. Upon overwinding and underwinding of DNA, its extension initially stays nearly constant, while its molecular torque increases linearly. At a critical supercoil density the molecule buckles and forms plectonemes, resulting in a decrease in the molecules extension and a saturation of the molecular torque. (**c**, **e**) For forces larger 1 pN the response of DNA is asymmetric: no buckling occurs for a negative number of turns (against the helical nature of DNA) and the corresponding torque reaches a plateau at -10 pN·nm [22, 55, 56]. Here, additional torsional stress is released by torque-induced melting of base pairs. At the highest stretching force (here 6.5 pN) no buckling occurs at all, since a transition of B-DNA to P-DNA occurs at $\sim$35 pN·nm. Data are for 7.9 kbp DNA measured with multiplexed magnetic torque tweezers with MyOne beads for forces $<$1 pN and M270 beads for forces $>$1 pN in TE-buffer (10 mM Tris and 1 mM EDTA) with 100 mM NaCl [46]. Figure adapted from Ref. [46].

beads' rotation about the vertical tether axis is unconstrained by the magnets. If precise alignment is achieved, beads will trace out a full doughnut shaped pattern in the (x, y)-plane, corresponding to a situation where the residual effect of the magnets on the rotational energy landscape is less than $\sim k_B T$, the thermal energy. The alignment is carried out as follows:

3.5.1 Coarse Alignment of the FOMT

1. From the geometry of the magnets used in FOMT, with an inner diameter of 2 mm, we expect the perfect aligned situation (only vertical field components, no radial field components, corresponding to a situation where the beads rotation about the vertical tether axis is unconstrained by the magnets) if the objective's main axis is in line with the magnets main axis.
2. To evaluate and improve alignment, we make use of the beads characteristic transverse fluctuations in the (x, y)-plane that trace out a doughnut-like shape if perfectly aligned (Fig. 2e).
3. In our instrument, we change the relative position of magnet and objective by moving the arm, which carries the magnet holder and the light emitting diode, in x and y direction using micrometer screws ($\sim$100 μm accuracy).
4. As a starting point we place the magnets such that we record maximal light intensity (on average) over the field of view ("light-based alignment").
5. At a fixed magnet height (typically 3 mm) we then record the fluctuations of beads and observe the fluctuation pattern in the (x, y)-plane for several times of the characteristic time of the system (*see* **Note 5**).
6. Focusing on the fluctuation pattern, one can maximize, i.e., optimize the number of aligned beads within a field of view by changing the relative position of magnet and objective using the micrometer screws ("coarse alignment").
7. For MyOne beads we find that this coarse grained method is often sufficient to have multiple aligned beads at the same time within the field of view (Fig. 4a).
8. In contrast, for M270 beads this coarse alignment is typically insufficient: We find no aligned bead, i.e., a bead that traces out a full doughnut in the (x, y)-fluctuations, in the field of view. Instead beads trace out only a segment of the doughnut. We achieve alignment of individual M270 beads by varying the x and y position of the magnet, independently, relative to the objective by steps of $\sim$100 μm.

3.5.2 Fine Alignment of the FOMT

1. To achieve a "perfect" aligned bead that fulfills the criteria to rotate about the tether axis unconstrained by the external magnets, it is best to focus on a single bead instead of many in parallel.

2. When plotting the recorded (x, y)-trace of a particular bead as a heat map, it is apparent that even a complete "doughnut" trace not necessarily suffices to have equal probability for all positions on the doughnut, indicating that there are still residual effects on the rotational energy landscape from the magnets (Fig. 4c shows a bead that is almost perfectly aligned).
3. To optimize the relative position of the bead and the magnet, one can translocate the flow cell itself using the micrometer screws of the base plates underneath the flow cell holder (or using a nano-positioning stage) with <10 μm accuracy ("fine tuning").
4. This finetuning is particularly relevant for larger beads, here M270 beads.
5. Note that sometimes coarse alignment is sufficient to align a single M270 bead.

3.6 DNA Torque Measurements

FOMT do not allow rotating the magnetic beads and, therefore, the DNA tethers cannot be supercoiled. MTT can be thought of as an extension of FOMT. To switch from FOMT to MTT a side magnet is added to the magnet holder that carries the stack of cylindrical magnets, as indicated in Fig. 1. For the side magnet, we use a cylindrical magnet with a diameter of 3 mm and a height of 6 mm (S-03-06-N, N-48, Supermagnete).

3.6.1 Optimization of the Instrument for Multiplexed Torque Measurements

1. The effect of the side magnet on the beads fluctuations in the (x, y)-plane is large: Displayed in Fig. 4b are the same beads as in Fig. 4a with the side magnet added to the FOMT configuration. All beads trace out a segment of the doughnut in the (x, y)-plane and are oriented toward the added side magnet.
2. MTT exert stretching forces on the molecular bead and allow tracking of the rotation angle of the bead, similar to FOMT, while additionally enable control of the twist of the DNA tether (Fig. 3a).
3. The magnitude of bead fluctuations is used to determine the stiffness of the rotational trap k_{ROT} (*see* Subheading 3.7, **step 10**).
4. k_{ROT} varies by 20% from bead-to-bead (*see* Supplementary Fig. S10 of Ref. [46]). This is understood from the anisotropy of the magnetic content within the particles [40].
5. To determine the trap stiffness of each individual bead in MTT, the (x, y)-fluctuations were measured for 600 s at each magnet height (3, 3.5, 4, 4.5 and 5 mm).
6. One can tune the effect of the side magnet on the beads by moving the magnets toward or away from the direction of the added side magnet [46]. This is of interest when performing multiplexed torque measurements, where the actual strength of

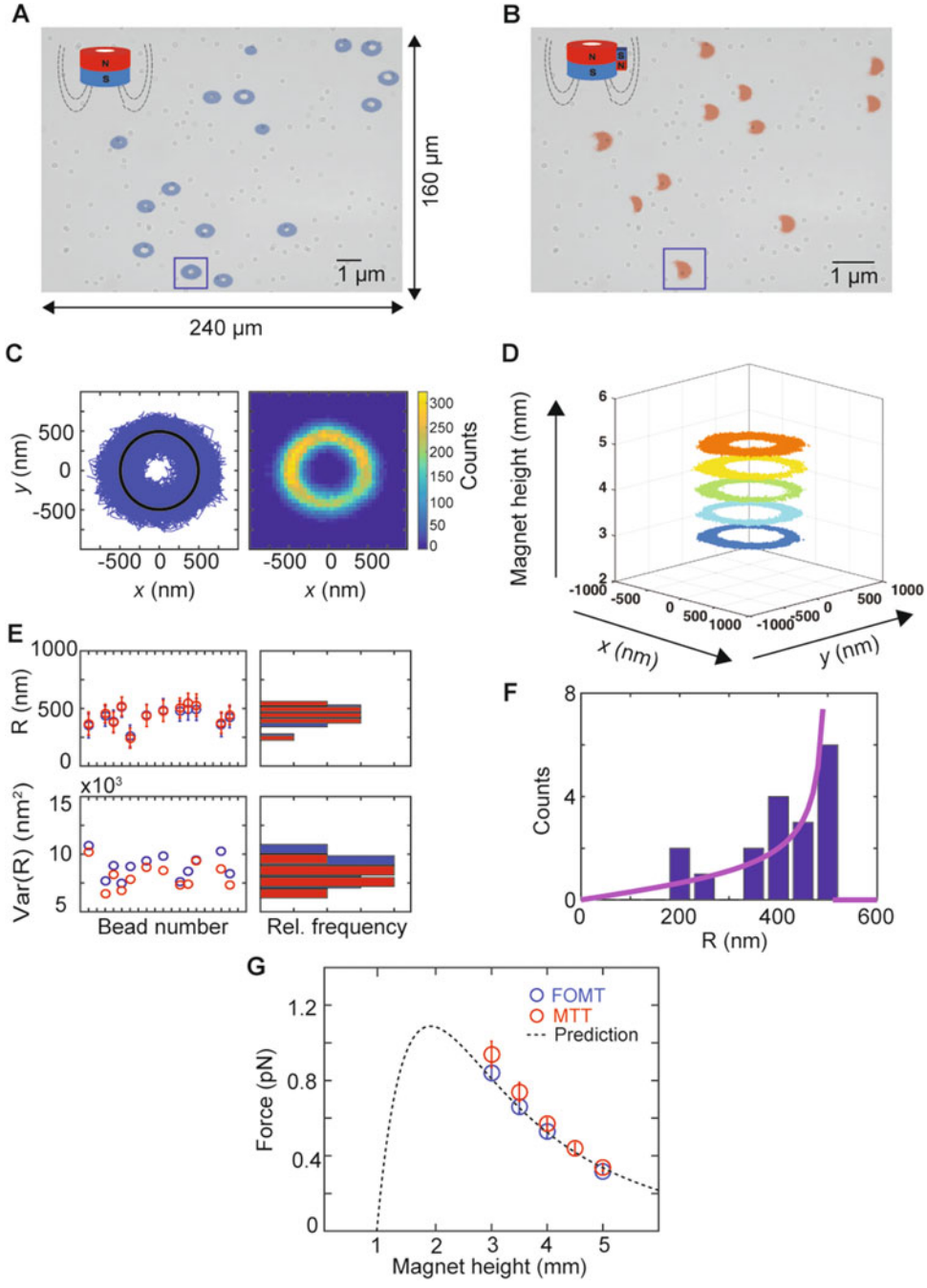

Fig. 4 Multiplexed FOMT and MTT and force calibration. (**a**) Multiplexed field of view in the FOMT geometry using 60× magnification and 7.9 kbp DNA attached to MyOne beads in PBS at 3 mm magnet height. Shown in blue are fluctuations of different beads in the (*x*, *y*)-plane. Fluctuations are all from the same 600 s recording and shown magnified compared to the camera image (1 µm scale bar gives the scale for the fluctuations; the size of the field of view is indicated on the sides). (**b**) Same field of view and same beads as in (a) (the number of beads was slightly reduced as some beads became unspecifically stuck to the surface). Upon adding a side magnet in the MTT configuration to the cylindrical magnet, the beads' (*x*, *y*)-fluctuations trace out arc-like

the trap stiffness plays a crucial role in determining molecular torque. There is an upper and a lower limit for k_{ROT}: on the one hand the trap needs to be strong enough such that the bead follows the rotation of the magnet (typically $k_{ROT} > 35$ pN·nm/rad), on the other hand the trap needs to be soft enough such that small changes in the shift in the equilibrium angle can be resolved (typically $k_{ROT} < 1000$ pN·nm/rad).

7. For multiplexed MTT measurements, the position of the magnet relative to the field of view can be varied (similar to "coarse alignment") such that the rotational trap stiffness that the beads experience are within these limits. Note that there is no need to perform a FOMT alignment prior to MTT measurements.

3.6.2 Protocol for Multiplexed Torque Measurements

1. During MTT measurements magnets are placed at a specific magnet height, i.e., stretching force, while the magnets are rotated.
2. If several forces should be measured, it is recommended to start with the highest stretching force to reduce unspecific interactions of the beads with the flow cell surface at lower stretching forces.
3. Typically starting at zero turns, the magnets are rotated against the helical nature of DNA, then back to zero, to a positive number of turns and back to zero.
4. Depending on tether length and the stretching force, the magnets are rotated several times in positive and negative direction of rotation (*see* Fig. 3 as an example for 7.9 kbp DNA attached with MyOne beads Fig. 3b, d, and attached to M270 beads, Fig. 3c, e).

Fig. 4 (continued) patterns shown in red. (**c**) (*x*, *y*)-fluctuations for one selected bead from the field of view in panel (a), tracked for 600 s. A histogram of the data, illustrated as a heat map (right panel), shows that the fluctuations of the bead are mostly uniformly distributed around the tether axis. (**d**) (*x*, *y*)-fluctuations of an aligned M270 bead attached to 7.9 kbp DNA in PBS at 3, 3.5, 4, 4.5, and 5 mm magnet height (blue to orange). The variance of the fluctuations of the bead around the doughnut radius *R* become larger with greater magnet distance, corresponding to lower stretching forces, while the mean of *R* stays constant (*see* also **Note 7**). (**e**) Mean doughnut radii *R* for the tethers shown in panel (a) and (b) in FOMT (blue circles) and MTT (red circles) geometry with the standard deviation as error bars. The close agreement between red and blue data points indicates that fitting the doughnut radius to time traces of thermal fluctuation in the FOMT or to traces during active magnet rotation in the MTT (*see* Subheading 3.7) gives the same result, within error. Corresponding variances of the radius in FOMT vs. MTT (same color code as before). (**f**) Histogram of doughnut radii *R* for the beads shown in panel A. The data are reasonably well described by a simple model based on spherical geometry (*see* **Note 8**; magenta line). (**e**) Forces computed from radial fluctuations in FOMT (blue circles) and MTT (red circles) for MyOne beads. Co-plotted is the force prediction in FOMT (dashed line) [27, 51]

5. Rotations are performed at 0.1 turn per second (typically in steps of two or five) to ensure that the bead follows the magnet rotation.
6. Data are recorded at a specific number of turns for several multiples of the characteristic time of the system at each measurement step, typically >50–100 s (*see* **Note 5**).
7. Data are typically recorded at 60 Hz.

3.7 Analysis of DNA Torque and Twist Measurements

1. The MT software saves the time, the (x, y, z)-position data, and the positions of the piezo and of both motors (translational and rotational) as text files.
2. The position of the translational motor and thus the magnet height above the flow cell can be used to determine the stretching force from a calibration measurement. For MyOne and M270 beads the bead-to-bead variation in stretching force is ~10% for a given setting of the magnets [51, 52]. Therefore, it is often sufficient to record a force-magnet height calibration (Fig. 4g) for a given setup configuration (*see* Subheading 3.8) and to then use the calibrated forces. We note, however, that other types of magnetic beads can be less homogeneous, requiring force calibration for every bead.
3. The position of the rotational motor gives the number of applied rotations and can be read out to identify the segments of the torque measurements where the magnets are rotating, *see* **step 5** below.
4. To calibrate the extension offset, i.e., to determine z-position where the beads touch the surface of the flow cell, it is recommended to record traces of each individual bead under condition where it contacts the surface (e.g., by tracking close to zero force) and to determine the corresponding z-value for subtraction in the following analysis of z.
5. In MTT, the segments of the measurements while rotating the magnets (*see* Subheading 3.6.2, **step 5** above) are used to (i) count and control the number of turns the bead rotated; (ii) fit a circle to the recorded (x, y)-positions in order to determine a radius and center position.
6. In FOMT, aligned beads trace out full circles, such that the circle fit can be performed on the whole recorded data set.
7. Using the fitted center position and radius of the doughnut in FOMT and MTT, one can transform the (x, y)-position of the bead to polar (r, Θ)-coordinates (Fig. 3a). *See* Eqs. 9–11 of Ref. [27] for details. We note that fitting a circle to the segments of traces where the bead is actively rotated in the MTT (*see* Subheading 3.6.2, **step 5** above) or to data where the bead traces out

a full "doughnut" by thermal fluctuation alone in the FOMT gives identical results, within experimental error (Fig. 4e).

8. In MTT, the segments of the measurements at a fixed number of rotations are used to determine changes in the equilibrium angle $\langle \Theta_N \rangle$ (Fig. 3a) and to monitor the DNA tether extension via the z-position of the bead.
9. The mean of the tracked angle positions is defined as equilibrium angle $\langle \Theta_N \rangle$.

   The beads fluctuations around the equilibrium angle $\langle \Theta \rangle$ are used to determine k_{ROT}:

$$k_{ROT} = k_B T / \mathrm{Var}(\Theta)$$

   where k_B is the Boltzmann constant and T the absolute temperature.
10. The shift in equilibrium angle after N turns is a direct measure for molecular torque (Fig. 3a, d, e):

$$\tau = -k_{ROT} \cdot (\langle \Theta_N \rangle - \langle \Theta_0 \rangle)$$

11. z is a direct measure of the extension of the molecule (Fig. 3b, c), after correcting for an z-offset (*see* Subheading 3.7, **step 4** above), i.e., after ensuring that the bead touching the surface is taking as the zero position.

3.8 Force Calibrations

While force calibration in conventional MT typically relies on analysis of the transverse (x, y)-fluctuations, in both FOMT and MTT the force calibration is based on analysis of the radial fluctuations after coordinate transformation from (x, y) to (r,Θ)-coordinates (*see* Subheading 3.7). Here, we compare force calibration in the FOMT with force calibration in the MTT.

1. In FOMT, we fit a circle to the radial thermal fluctuations of the bead, while in MTT we fit a circle to the recorded trace of the bead when turning the magnet to determine a center point and such transfer the data to polar coordinates (here: six rotations at 0.1 turn per second).
2. We performed force calibrations (F) similar to Ref. [27] for different magnet heights z_{mag}, where l is the measured tether length and $\mathrm{Var}(R)$ the variance of radial fluctuations:

$$F = k_B T \cdot l / \mathrm{Var}(R)$$

3. We use the recorded transverse fluctuations in x and y to determine the radius R and the recorded z trace to calculate the tether length l.
4. Both methods are in good agreement (Fig. 4g) allowing us to directly perform force calibrations in MTT or to use existing

FOMT force calibrations for torque measurements (*see* **Notes 1** and **6**). The force calibrations based on the radial fluctuations are, in addition, in good agreement with prediction from magnetic field and bead magnetization calculations [27, 51] (Fig. 4g, dashed line).

4 Notes

1. The stretching force is dependent on the beads' magnetization (in turn determined by the size and type of the beads) and on the magnetic field and its gradient [51]. For both MyOne and M270 beads, the bead-to-bead variability in the force is ~10%. The inhomogeneity in force across the field of view is <10% in the MT configurations described here [46]. The inhomogeneity in the stiffness of the rotational trap in MTT measurements is about 20% [40, 46].
2. In particular if the biological system is sensitive to buffer conditions, it is recommended to perform a buffer exchange for the magnetic beads prior to incubation with the DNA, by using a magnet pipette aid to pull the magnetic beads to one side of the Eppendorf tube so that one can easily remove the solution with a pipette and add the desired measurement buffer. Here, we typically use PBS for the buffer exchange.
3. In conventional MT, FOMT and MTT, the set of magnets are assembled in a magnet holder mount made from aluminum that is itself not magnetic. The magnet holder is fixed to the instrument via a screw. After bringing the translational motor to its maximal height, which is usually 2 cm above the flow cell surface, it is easy to manually replace the magnet holder with another magnet configuration. For fast exchange, it is convenient to place each magnet configuration in its own magnet holder.
4. In the FOMT and MTT configurations field gradients change signs, such that at a certain distance (<1 mm for the magnets described here that feature a 2 mm diameter aperture) of the magnet to the flow cell the magnet exerts pushing instead of pulling forces (Fig. 4g) [27, 51].
5. For high-resolution measurements (e.g., of molecular torques in the MTT or of angular steps in the FOMT) the overall measurement time T_{meas} should be—ideally—significantly larger than the characteristic time of the system τ_{c}. The characteristic time of the system is generally given by the friction coefficient γ divided by the trap stiffness k. For the rotational degree of freedom, the friction coefficient is $\gamma_{\mathrm{ROT}} \approx 140\pi\eta R^3$ (the exact formula is given as Eq. 18 in Ref. [27]) and

$k_{ROT} = k_B \cdot T/\mathrm{Var}(\Theta)$, where η is the viscosity of the solution ($\eta \approx 0.001$ Pa·s for aqueous buffers). In the FOMT, $k_{ROT} = k_B \cdot TC/L_C$, where C is the torsional persistence length (≈50–100 nm, depending on the stretching force) and L_C the contour length of the employed DNA molecule [27]. In particular for long DNA molecules and large beads, characteristic times in the FOMT can be very long (e.g., $\tau_c \sim 1000$ s for M270 beads and the 7.9 kbp DNA), which severely limits the ability to detect steps in the angular coordinate, since steps can only be reliably detected if they occur more slowly than τ_c. For small beads ($R_{bead} \leq 0.5$ μm) and short DNA tethers ($L_C \leq 0.5$ μm) characteristic times in the FOMT are reduced to ≤15 s. The MTT characteristic times are generally much shorter than in the FOMT, due to the (much) higher rotational trap stiffness.

6. While the fitted radius in FOMT and MTT is similar, the beads fluctuations, i.e., the variance of the radius is slightly smaller in MTT, which leads to an overestimation of the forces in MTT compared to FOMT. This is understood as the fluctuations while rotation the magnet (as used in MTT) are smaller than fluctuations in FOMT.
7. Figure 4d: the position of the magnet was adjusted when changing the magnet height in order to measure full circle fluctuations ("*fine tuning*"). In general, the magnet alignment in FOMT is so sensitive that significant changes in the magnet height require realignment of the (x, y)-position of the magnets.
8. The paramagnetic beads used in MT experiments have a preferred magnetization axis [40, 53], $\vec{m}_0$, that aligns with the external field (Fig. 2). A DNA attachment at the bottom of the bead in conventional MT (where the magnetic field is horizontal) corresponds to an attachment at the side of the bead in FOMT or MTT (where the field is (nearly) vertical); in both cases the DNA is attached at the "equator" of the bead relative to the preferred magnetization axis that defines the "poles" (this is the situation shown schematically in Fig. 2). Similarly, for an attachment of the DNA at one of the poles, the DNA would be attached to the bead at the side in conventional MT and at the bottom (or top) in FOMT or MTT. Since the beads are typically uniformly functionalized and DNA–bead coupling is carried out in free solution, we do not control the attachment point of the DNA to the bead. However, attachment at or near the equator is much more likely than attachment at or near one of the poles due to spherical geometry. The area per polar angle θ segment $\mathrm{d}A = 4\pi R_{bead}{}^2 \cdot \sin(\theta)\mathrm{d}\theta$ is much larger at the equator (where $\theta \sim \pi/2$ such that $\sin(\theta) \sim 1$) compared to the poles (with $\theta \sim 0$ or π such that $\sin(\theta) \sim 0$). From this argument

follows that, assuming random attachment anywhere on the bead's surface, the probability to observe a given doughnut radius R is proportional to $P \sim R/R_{\mathrm{bead}}[1-(R/R_{\mathrm{bead}})^2]^{-1/2}$, in good agreement with the experimental observations (Fig. 4f).

Acknowledgments

We thank Jelle van der Does for help with instrument development, Susanne Hage for help with development of the DNA construct, Philipp Walker for instrument construction and useful discussions, the Rief chair at the TU Munich for use of the laser cutter, and the German Research Foundation (DFG) via Sonderforschungbereich SFB 863 "Forces in Biomolecular Systems" for funding.

References

1. Bryant Z, Oberstrass FC, Basu A (2012) Recent developments in single-molecule DNA mechanics. Curr Opin Struct Biol 22:304–312
2. Lipfert J, van Oene MM, Lee M, Pedaci F, Dekker NH (2015) Torque spectroscopy for the study of rotary motion in biological systems. Chem Rev 115:1449–1474
3. Neuman KC, Nagy A (2008) Single-molecule force spectroscopy: optical tweezers, magnetic tweezers and atomic force microscopy. Nat Methods 5:491–505
4. Manosas M, Meglio A, Spiering MM, Ding F, Benkovic SJ, Barre F-X et al (2010) Magnetic tweezers for the study of DNA tracking motors. Methods Enzymol 475:297–320
5. Strick TR, Allemand JF, Bensimon D, Bensimon A, Croquette V (1996) The elasticity of a single supercoiled DNA molecule. Science 271:1835–1837
6. Gosse C, Croquette V (2002) Magnetic tweezers: micromanipulation and force measurement at the molecular level. Biophys J 82:3314–3329
7. te Velthuis AJW, Kerssemakers JWJ, Lipfert J, Dekker NH (2010) Quantitative guidelines for force calibration through spectral analysis of magnetic tweezers data. Biophys J 99:1292–1302
8. Lansdorp BM, Saleh OA (2012) Power spectrum and Allan variance methods for calibrating single-molecule video-tracking instruments. Rev Sci Instrum 83:025115
9. Daldrop P, Brutzer H, Huhle A, Kauert DJ, Seidel R (2015) Extending the range for force calibration in magnetic tweezers. Biophys J 108:2550–2561
10. Strick TR, Allemand JF, Bensimon D, Croquette V (2000) Stress-induced structural transitions in DNA and proteins. Annu Rev Biophys Biomol Struct 29:523–543
11. Abels JA, Moreno-Herrero F, Van Der Heijden T, Dekker C, Dekker NH (2005) Single-molecule measurements of the persistence length of double-stranded RNA. Biophys J 88:2737–2744
12. Herrero-Galán E, Fuentes-Perez ME, Carrasco C, Valpuesta JM, Carrascosa JL, Moreno-Herrero F et al (2013) Mechanical identities of RNA and DNA double helices unveiled at the single-molecule level. J Am Chem Soc 135:122–131
13. Lipfert J, Klijnhout S, Dekker NH (2010) Torsional sensing of small-molecule binding using magnetic tweezers. Nucleic Acids Res 38:7122–7132
14. Salerno D, Brogioli D, Cassina V, Turchi D, Beretta GL, Seruggia D et al (2010) Magnetic tweezers measurements of the nanomechanical properties of DNA in the presence of drugs. Nucleic Acids Res 38:7089–7099
15. Wang Y, Schellenberg H, Walhorn V, Toensing K, Anselmetti D (2017) Binding mechanism of fluorescent dyes to DNA characterized by magnetic tweezers. Mater Today Proc 4:S218–S225
16. Vilfan ID, Lipfert J, Koster DA, Lemay SG, Dekker NH (2009) Magnetic tweezers for single molecule measurements. Springer, New York, NY

17. Carrasco C, Dillingham MS, Moreno-Herrero F (2014) Single molecule approaches to monitor the recognition and resection of double-stranded DNA breaks during homologous recombination. DNA Repair (Amst) 20:119–129
18. Dulin D, Berghuis BA, Depken M, Dekker NH (2015) Untangling reaction pathways through modern approaches to high-throughput single-molecule force-spectroscopy experiments. Curr Opin Struct Biol 34:116–122
19. Berghuis BA, Köber M, van Laar T, Dekker NH (2016) High-throughput, high-force probing of DNA-protein interactions with magnetic tweezers. Methods 105:90–98
20. Ordu O, Lusser A, Dekker NH (2016) Recent insights from in vitro single-molecule studies into nucleosome structure and dynamics. Biophys Rev 8:33–49
21. Hodeib S, Raj S, Manosas M, Zhang W, Bagchi D, Ducos B et al (2016) Single molecule studies of helicases with magnetic tweezers. Methods 105:3–15
22. Bryant Z, Stone MD, Gore J, Smith SB, Cozzarelli NR, Bustamante C (2003) Structural transitions and elasticity from torque measurements on DNA. Nature 424:338–341
23. Gore J, Bryant Z, Stone MD, Nöllmann M, Cozzarelli NR, Bustamante C (2006) Mechanochemical analysis of DNA gyrase using rotor bead tracking. Nature 439:100–104
24. Lebel P, Basu A, Oberstrass FC, Tretter EM, Bryant Z (2014) Gold rotor bead tracking for high-speed measurements of DNA twist, torque and extension. Nat Methods 11:456–462
25. Oberstrass FC, Fernandes LE, Bryant Z (2012) Torque measurements reveal sequence-specific cooperative transitions in supercoiled DNA. Proc Natl Acad Sci U S A 109:6106–6111
26. Vlijm R, Lee M, Lipfert J, Lusser A, Dekker C, Dekker NH (2015) Nucleosome assembly dynamics involve spontaneous fluctuations in the handedness of Tetrasomes. Cell Rep 10:216–225
27. Lipfert J, Wiggin M, Kerssemakers JWJ, Pedaci F, Dekker NH (2011) Freely orbiting magnetic tweezers to directly monitor changes in the twist of nucleic acids. Nat Commun 2:439–439
28. Lee M, Lipfert J, Sanchez H, Wyman C, Dekker NH (2013) Structural and torsional properties of the RAD51-dsDNA nucleoprotein filament. Nucleic Acids Res 41:7023–7030
29. Harada Y, Ohara O, Takatsuki A, Itoh H, Shimamoto N, Kinosita K (2001) Direct observation of DNA rotation during transcription by *Escherichia coli* RNA polymerase. Nature 409:113–115
30. Basu A, Schoeffler AJ, Berger JM, Bryant Z (2012) ATP binding controls distinct structural transitions of *Escherichia coli* DNA gyrase in complex with DNA. Nat Struct Mol Biol 19:538–546
31. Celedon A, Nodelman IM, Wildt B, Dewan R, Searson P, Wirtz D et al (2009) Magnetic tweezers measurement of single molecule torque. Nano Lett 9:1720–1725
32. Celedon A, Wirtz D, Sun S (2010) Torsional mechanics of DNA are regulated by small-molecule intercalation. J Phys Chem B 114:16929–16935
33. Lipfert J, Kerssemakers JWJ, Jager T, Dekker NH (2010) Magnetic torque tweezers: measuring torsional stiffness in DNA and RecA-DNA filaments. Nat Methods 7:977–980
34. Lipfert J, Kerssemakers JJW, Rojer M, Dekker NH (2011) A method to track rotational motion for use in single-molecule biophysics. Rev Sci Instrum 82:103707
35. Janssen XJA, Lipfert J, Jager T, Daudey R, Beekman J, Dekker NH (2012) Electromagnetic torque tweezers: a versatile approach for measurement of single-molecule twist and torque. Nano Lett 12:3634–3639
36. Mosconi F, Allemand JF, Croquette V (2011) Soft magnetic tweezers: a proof of principle. Rev Sci Instrum 82:034302
37. Kauert DJ, Kurth T, Liedl T, Seidel R (2011) Direct mechanical measurements reveal the material properties of three-dimensional DNA origami. Nano Lett 11:5558–5563
38. Lipfert J, Skinner GM, Keegstra JM, Hensgens T, Jager T, Dulin D et al (2014) Double-stranded RNA under force and torque: similarities to and striking differences from double-stranded DNA. Proc Natl Acad Sci U S A 111:15408–15413
39. Lipfert J, Lee M, Ordu O, Kerssemakers JWJ, Dekker NH (2014) Magnetic tweezers for the measurement of twist and torque. J Vis Exp 19 (87). https://doi.org/10.3791/51503
40. van Oene MM, Dickinson LE, Pedaci F, Köber M, Dulin D, Lipfert J et al (2015) Biological magnetometry: torque on superparamagnetic beads in magnetic fields. Phys Rev Lett 114:218301. https://doi.org/10.1103/PhysRevLett.114.218301
41. van Oene MM, Dickinson LE, Cross B, Pedaci F, Lipfert J, Dekker NH (2017) Applying torque to the *Escherichia coli* flagellar motor using magnetic tweezers. Sci Rep 7:43285

42. Nord AL, Gachon E, Perez-Carrasco R, Nirody JA, Barducci A, Berry RM et al (2017) Catch bond drives stator mechanosensitivity in the bacterial flagellar motor. Proc Natl Acad Sci U S A 114:12952–12957
43. Ribeck N, Saleh OA (2008) Multiplexed single-molecule measurements with magnetic tweezers. Rev Sci Instrum 79:094301
44. De Vlaminck I, Henighan T, van Loenhout MTJ, Pfeiffer I, Huijts J, Kerssemakers JWJ et al (2011) Highly parallel magnetic tweezers by targeted DNA tethering. Nano Lett 11:5489–5493
45. Cnossen JP, Dulin D, Dekker NH (2014) An optimized software framework for real-time, high-throughput tracking of spherical beads. Rev Sci Instrum 85:103712
46. Kriegel F, Ermann N, Forbes R, Dulin D, Dekker NH, Lipfert J (2017) Probing the salt dependence of the torsional stiffness of DNA by multiplexed magnetic torque tweezers. Nucleic Acids Res 45:5920–5929
47. Nomidis SK, Kriegel F, Vanderlinden W, Lipfert J, Carlon E (2017) Twist-bend coupling and the torsional response of double-stranded DNA. Phys Rev Lett 118:217801
48. Dulin D, Vilfan ID, Berghuis BA, Hage S, Bamford DH, Poranen MM et al (2015) Elongation-competent pauses govern the Fidelity of a viral RNA-dependent RNA polymerase. Cell Rep 10:983–992
49. van Loenhout MTJ, Kerssemakers JWJ, De Vlaminck I, Dekker C (2012) Non-bias-limited tracking of spherical particles, enabling Nanometer resolution at low magnification. Biophys J 102:2362–2371
50. Lipfert J, Koster DA, Vilfan ID, Hage S, Dekker NH (2009) Single-molecule magnetic tweezers studies of type IB topoisomerases. Methods Mol Biol 582:71–89
51. Lipfert J, Hao X, Dekker NH (2009) Quantitative modeling and optimization of magnetic tweezers. Biophys J 96:5040–5049
52. De Vlaminck I, Henighan T, van Loenhout MT, Burnham DR, Dekker C (2012) Magnetic forces and DNA mechanics in multiplexed magnetic tweezers. PLoS One 7:e41432
53. Klaue D, Seidel R (2009) Torsional stiffness of single Superparamagnetic microspheres in an external magnetic field. Phys Rev Lett 102:028302
54. Kriegel F, Ermann N, Lipfert J (2017) Probing the mechanical properties, conformational changes, and interactions of nucleic acids with magnetic tweezers. J Struct Biol 197:26–36
55. Mosconi F, Allemand JF, Bensimon D, Croquette V (2009) Measurement of the torque on a single stretched and twisted DNA using magnetic tweezers. Phys Rev Lett 102:078301
56. Sheinin MY, Forth S, Marko JF, Wang MD (2011) Underwound DNA under tension: structure, elasticity, and sequence-dependent Behaviors. Phys Rev Lett 107:108102